Draft Manuscript for Review

Depths in a day - A new era of rapid-response Raman-based barometry using fluid inclusions

1   **Depths in a day - A new era of rapid-response Raman-based**

2   **barometry using fluid inclusions.**

3   Running title: Depths in a day – a new era of rapid response barometry

4

5   Charlotte L. DeVitre[1]*, Penny E. Wieser[1], Alexander T. Bearden[1], Araela Richie[1], Berenise

6   Rangel[1], Matthew LM Gleeson[1], John Grimsich[1], Kendra J. Lynn[2], Drew T. Downs[2],

7   Natalia I. Deligne[2], and Katherine M. Mulliken[2]

8   [1] Earth and Planetary Sciences, University of California, Berkeley, CA 94270, USA

9   [2] U. S. Geological Survey, Hawaiian Volcano Observatory, Hilo, HI 96720, USA

10   * Corresponding author: Charlotte L. DeVitre cl.devitre@gmail.com

11   ⓘ ORCiD (CLD): 0000-0002-7167-7997

12   ⓘ ORCiD (KJL): 0000-0001-7886-4376

13   ⓘ ORCiD (DTD): 0000-0002-9056-1404

14   ⓘ ORCiD (NID): 0000-0001-9221-8581

15   Word count: Abstract 70, Main1705

16   **Abstract**

17   Rapid-response petrological monitoring is a major advance for volcano

18   observatories to build and validate models of the plumbing systems that supply eruptions

19   in near-real-time. Our rapid-response analysis of tephra from the September 2023 eruption

20   of Kīlauea shows that Raman analyses of fluid inclusions can robustly determine magma

21   reservoir depths within a day of receiving samples – a transformative timescale for decision

22   making that has not previously been achieved by petrological methods.

23   **Keywords:** Fluid Inclusions; Geobarometry; Raman Spectroscopy; Rapid Response;

24   Volcano Monitoring

25

26

Main Text

Volcano observatories increasingly use data collected from erupted lava and tephra samples in near-real-time to obtain information about the magmatic plumbing system to help inform decision making during volcanic crises (Gansecki *et al.*, 2019; Re *et al.*, 2021; Pankhurst *et al.*, 2022). Most work so far has focused on the chemistry of erupted lavas and crystal cargoes (Pankhurst *et al.*, 2022) to gain insight into changing melt composition and rheological properties (e.g., Gansecki *et al.*, 2019). However, up until now, petrological monitoring has been unable to address the high-priority question– '*Where is the magma coming from?*' (Re *et al.*, 2021). At well-monitored volcanoes, such information can be used to draw analogies to previous eruptive episodes associated with specific storage reservoirs (e.g., vigour, pathway, or length of eruption), and to help interpret geophysical signals of ongoing activity. At poorly-monitored volcanoes, where there may be no prior constraints on magma storage geometry (Wieser *et al.*, 2023b), depths of storage are a vital parameter to begin interpreting new eruptive activity. Melt inclusion (MI) barometry, a widely popular petrological method to determine storage depths from volatile contents, takes months to years to complete (Re *et al.*, 2021). While mineral barometry could be implemented faster (only requiring electron probe microanalysis (EPMA) measurements on eruptive minerals), it is imprecise (Wieser *et al.*, 2023a), and therefore would only be able to constrain magma storage to very broad depths (e.g., stored in the crust vs. below the Moho). This technique has particularly poor applicability at active volcanoes such as Kīlauea or Mauna Loa, where a precision of 1–2

49   km is needed to distinguish between storage reservoirs (Baker and Amelung, 2012;

50   Anderson and Poland, 2016).

51   Recent developments have shown that Raman-based barometry of CO_2-rich fluid

52   inclusions (FI) provides an alternative to popular petrological barometers, with much

53   smaller uncertainties than mineral barometry, and requiring far less time and resources than

54   MI analyses (Dayton *et al.*, 2023; DeVitre and Wieser, 2023). This method uses spectral

55   features of CO_2 fluids to calculate a CO_2 density using an instrument specific calibration

56   (DeVitre *et al.*, 2021). Along with an estimate of entrapment temperature, this density is

57   converted into an entrapment pressure using a CO_2 Equation of State (EOS). Pressures are

58   converted to depths through an estimate of crustal density. However, there has previously

59   been no rigorous assessment of how quickly FI depths can be obtained from erupted

60   material, and whether these timescales are short enough to have use as a real-time

61   monitoring tool.

62   The eruption onset of Kīlauea volcano on September 10, 2023 provided an

63   unprecedented opportunity to test the validity of this method during a response, given that

64   depths of the main magma storage regions at this volcano have been well constrained by

65   various independent geophysical and petrological methods, including prior FI barometry

66   (DeVitre and Wieser, 2023). Tephra samples representing the first ~14 hours of the

67   September 2023 eruption were collected by Hawaiian Volcano Observatory (HVO)

68   geologists on September 12 and mailed to UC Berkeley on September 15th (Fig. 1).

69   Our simulation started on September 20 at 9 am PST (Day 1), the morning after

70   sample receipt (Fig. 1). We used a production-line style workflow involving two

71   undergraduates, a 1st year graduate student, a post-doc, and an assistant professor, with

* The use of trade names does not signify endorsement by the U.S. Geological Survey.

72   stations for crushing and sieving, mineral picking, FI preparation, sample cataloguing, and

73   analysis. The first steps were to crush and sieve tephra, pick olivine crystals (size fractions

74   0.5-1 and 1-2 mm) crystals, and begin mounting crystals in CrystalBond[TM*] to search for

75   FI. By 2 pm PST (5 hrs into the simulation), we had collected our first Raman spectra. By

76   ~7 pm PST, we had processed the spectra from 16 FI to get CO_2 densities using a

77   calibration relating CO_2 density to Fermi Diad separation (DeVitre and Wieser (2023),

78   DeVitre et al. 2021). CO_2 densities were converted into pressures using the EOS of Span

79   and Wagner, 1996), assuming an entrapment temperature of 1150 ˚C. Pressures were

80   converted into depths using the crustal density model of Ryan, (1987) parameterized by

81   Lerner *et al.* (2021). We shared the resulting histogram (Fig 2a) of storage depths with

82   HVO collaborators showing that crystals, and thus magma, were likely coming from the

83   shallower Halemaʻumaʻu reservoir of Kīlauea (HMM on Fig. 2a–b). It worthwhile to note

84   that the number of FI reported on Day 2 is comparable to many melt inclusion studies,

85   which often aim for ~20 MI per sample but frequently report fewer (e.g., Lerner *et al.*,

86   2021) reported 14 MI with sufficient data – that is MI glass total volatile contents and major

87   element compositions - to produce saturation pressures for the LERZ eruption of 2018).

88   We also had an additional ~20 FI fully prepared and catalogued for analysis by the end of

89   Day 1.

90   On Day 2, these 20 FI were analysed, while supplementary FI were prepared and

91   catalogued. After analysis of ~15 crystals hosting FI, these crystals were passed from the

92   Raman to a workstation where they were removed from CrystalBond[TM] and placed on tape

93   to make an epoxy mount. Epoxy was poured at the end of the day. By ~8:30 pm PST on

94   Day 2, we shared an updated histogram of 46 FI pressures and depths, confirming the

* The use of trade names does not signify endorsement by the U.S. Geological Survey.

95   dominant contribution of the Halemaʻumaʻu reservoir (Fig. 2a and c). On Day 3, while

96   waiting for the epoxy to fully set, we finished analysing prepared FI. Then we polished the

97   mount and began cataloguing the regions of crystals on which to perform energy-dispersive

98   spectroscopy (EDS). On Day 4, olivine forsterite contents (Fo = 100*Mg/(Mg+Fe) molar)

99   were determined by EDS, providing a framework to further interpret the plumbing system

100   (Fig. 2d). The Fo content of an olivine is a function of MgO and FeO in the liquid and the

101   Ol-Liq partitioning coefficient (K_D). Thus, the Fo contents of the host olivine close to each

102   FI can be used to assess the calculated storage depth in its broader petrographic context

103   (e.g., distinguishing high-Fo olivines which crystallize from more primitive melts from low

104   Fo olivines forming in more evolved melts). This olivine forsterite content can also be used

105   to estimate the likely entrapment temperature of each fluid inclusion (see DeVitre and

106   Wieser, 2023) for performing EOS calculations, rather than having to use a uniform

107   temperature as on Day 1-2.

108   Our results clearly show that the majority of FI were entrapped at ~1–2 km below

109   the surface (Fig. 2d), which aligns well with the depths of the Halemaʻumaʻu reservoir

110   interpreted from geophysics (Baker and Amelung, 2012; Anderson and Poland, 2016;

111   Anderson *et al.*, 2019), MI barometry (Lerner *et al.*, 2021; Wieser *et al.*, 2021), and FI

112   barometry (DeVitre and Wieser, 2023). While the greater number of analyses from data

113   processed on Day 2 and Day 4 certainly enhance the story, it is notable that depths

114   calculated on Day 1 fall within final proposed storage reservoir depths. Rapid EDS

115   analyses of olivine Fo contents close to each FI reveal that olivine crystals grew from a

116   wide range of melt compositions. It is interesting to note that FI in the cores of high-Fo

117   (e.g., >86) olivine crystals return pressures indicative of the shallower Halemaʻumaʻu

118   reservoir since it has been suggested in previous eruptions that these high-Fo olivine

119   crystals predominantly grow in the deeper South Caldera reservoir (SC on Fig. 2a), where

120   high MgO melts are thought to reside (Helz *et al.*, 2014; Pietruszka *et al.*, 2015, 2018;

121   Wieser *et al.*, 2019). We suggest three possible scenarios to explain the relatively shallow

122   pressures documented in high-Fo olivine crystals:

123   1) FI in high-Fo olivine crystals were entrapped within the South Caldera reservoir and then

124   transported into the Halemaʻumaʻu reservoir, where the fluid inclusions re-equilibrated to

125   lower pressures prior to eruption over shorter timescales than would be required to reset

126   the host Fo content.

127   2) High-MgO melts were injected into the Halemaʻumaʻu reservoir, where high-Fo olivine

128   crystallized and trapped FI at shallow depths.

129   3) Complex skeletal growth of olivine crystals during extensive undercooling (e.g.,

130   (Welsch *et al.*, 2013) could mean that high-Fo olivine cores, which initially grew in the SC

131   reservoir texturally evolved and trapped lower pressure FI in the Halemaʻumaʻu reservoir.

132   We think that scenario 1 is unlikely given the that FI from the 2018 lower East Rift

133   Zone eruption appear not to have re-equilibrated despite stalling in the Halemaʻumaʻu

134   reservoir for up to 2 years (DeVitre and Wieser, 2023; Mourey *et al.*, 2023), and our models

135   of FI re-equilibration indicate <10% change in pressure over this time period. Current data

136   does not allow us to resolve scenario 2 vs 3, but this eruption could provide an opportunity

137   to explore this further (e.g., through detailed Phosphorous mapping in olivine around FI).

138   Regardless of the exact mechanism, our FI pressures indicate that erupted crystal cargo

139   experienced storage at Halemaʻumaʻu reservoir depths prior to eruption, and thus this was

140   the most probable reservoir supplying magma to the surface in the Sept 2023 eruption.

141   This simulation shows that Raman-based FI barometry has significant potential for

142   rapid-response petrological monitoring globally. It could be applied to any CO_2-rich

143   volcanic system – which includes numerous hazardous and frequently active volcanic

144   regions worldwide (e.g., Galápagos, Réunion, Azores, Canary Islands, Iceland, Cabo

145   Verde). The resources and personnel required are modest. Sample preparation was carried

146   out using transmitted-reflected light microscopes from the University of California

147   teaching collection, only using a research-grade microscope for sample cataloguing.

148   Raman spectrometers are widely available at many universities, given that it is a popular

149   technique in many other fields, such as material sciences, physics, chemistry, and biology,

150   and the W-filament SEM used for EDS analyses to get olivine Fo contents has been around

151   for 15 years (See Supplementary Information S1 Appendix).

152   This simulation also enabled us to identify several 'bottlenecks' in this rapid-

153   response workflow (yellow stars, Fig, 1, see Supplementary Information S1 Appendix for

154   further details) so that we could determine depths even faster during future eruptions:

155   1) No courier services ship packages out of Hilo, Hawai'i over the weekend, and

156   estimated delivery days are not reliable.

157   2)   The epoxy took 18 hours to cure enough for polishing (vs. 8 hours on the datasheet).

158   Faster curing epoxies can be used to eliminate this delay.

159   3) We spent significant time cataloguing samples on a research-grade microscope to

160   help navigate on the Raman microscope, but later realized that smartphone cameras

161   with teaching microscopes would have worked faster.

162   Overall, we have demonstrated that a modest-sized research group with prior teaching and

163   class commitments working without overnight shifts can obtain pressures on relevant

* The use of trade names does not signify endorsement by the U.S. Geological Survey.

164   timelines for understanding volcanic plumbing systems during periods of unrest. This

165   technique adds valuable quantitative storage depth information that expands on HVO's

166   routine near-real-time chemical monitoring with bulk rock ED-XRF(Gansecki *et al.*, 2019).

167   In a true eruptive crisis, magma storage depths could be obtained even faster by removing

168   bottlenecks 1–3, implementing overnight shift work, and requesting teaching release and class

169   absences for students.

170

Author contributions

172   Author contributions for lab work are shown on Fig. 1. CD and PW wrote the paper. CD,

173   PW, AR, BR, and AB prepared tephra, picked olivine, found FIs, catalogued them,

174   mounted them, and conducted Raman analyses. CD and PW performed all spectral fitting,

175   data processing, and figure making, with schematic illustrations shown in Fig. 1 from AB.

176   JG developed the Mg/Fe calibration for the EDS detector and MG performed EDS analyses

177   with help from JG. KJL, DTD, NID and KMM collected samples, processed them in Hilo,

178   and provided eruption context. KJL and DD prepared the glass mount and did the EMPA

179   analyses.

180

Acknowledgements

185

Data availability

187   All data are made available in the Supplementary Information associated with the

188   publication. We include detailed materials and methods (S1 Appendix), complete

189   processed Dataset (S2 Dataset), a compilation of microphotographs of the FI and crystals

190   (S3 FI Image Compilation) and a record of emails and tracking receipts related to the

191   samples, data sharing and manuscript submission (S4 Email and tracking record). All raw

192   data   and   Jupyter   notebooks   are   also   stored   on   Github

193   (https://github.com/cljdevitre/2023_Kilauea-rapid-response-simulation).   The   Github

194   repository will be archived on Zenodo upon acceptance.

195

References

197

198   Anderson, K. R., Johanson, I. A., Patrick, M. R., Gu, M., Segall, P., Poland, M. P., Montgomery-
199   Brown, E. K. & Miklius, A. (2019). Magma reservoir failure and the onset of caldera
200   collapse at Kīlauea Volcano in 2018. *Science*. American Association for the
201   Advancement of Science **366**, eaaz1822.

202   Anderson, K. R. & Poland, M. P. (2016). Bayesian estimation of magma supply, storage, and
203   eruption rates using a multiphysical volcano model: Kīlauea Volcano, 2000–2012. *Earth*
204   *and Planetary Science Letters* **447**, 161–171.

205   Baker, S. & Amelung, F. (2012). Top-down inflation and deflation at the summit of Kīlauea
206   Volcano, Hawaiʻi observed with InSAR. *Journal of Geophysical Research: Solid Earth*
207   **117**.

208   Dayton, K. *et al.* (2023). Deep magma storage during the 2021 La Palma eruption. *Science*
209   *Advances*. American Association for the Advancement of Science **9**, eade7641.

210   DeVitre, C. L., Allison, C. M. & Gazel, E. (2021). A high-precision CO2 densimeter for Raman
211   spectroscopy using a Fluid Density Calibration Apparatus. *Chemical Geology* **584**,
212   120522.

213 DeVitre, C. L. & Wieser, P. (2023). Reliability of Raman analyses of CO2-rich fluid inclusions as
214   a rapid barometer at Kīlauea. EarthArXiv.

215 Gansecki, C., Lee, R. L., Shea, T., Lundblad, S. P., Hon, K. & Parcheta, C. (2019). The tangled
216   tale of Kīlauea's 2018 eruption as told by geochemical monitoring. *Science*. American
217   Association for the Advancement of Science **366**, eaaz0147.

218 Helz, R. T., Clague, D. A., Sisson, T. W. & Thornber, C. R. (2014). *Petrologic insights into
219   basaltic volcanism at historically active Hawaiian volcanoes*. *Characteristics of
220   Hawaiian volcanoes*. US Geological Survey, Professional Papers, 237–294.

221 Lerner, A. H. *et al.* (2021). The petrologic and degassing behavior of sulfur and other magmatic
222   volatiles from the 2018 eruption of Kīlauea, Hawai'i: melt concentrations, magma
223   storage depths, and magma recycling. *Bulletin of Volcanology*. Springer **83**, 1–32.

224 Mourey, A. J., Shea, T., Costa, F., Shiro, B. & Longman, R. J. (2023). Years of magma intrusion
225   primed Kīlauea Volcano (Hawai'i) for the 2018 eruption: evidence from olivine diffusion
226   chronometry and monitoring data. *Bulletin of Volcanology* **85**, 18.

227 Pankhurst, M. J. *et al.* (2022). Rapid response petrology for the opening eruptive phase of the
228   2021 Cumbre Vieja eruption, La Palma, Canary Islands. *Volcanica* **5**, 1–10.

229 Pietruszka, A. J., Heaton, D. E., Marske, J. P. & Garcia, M. O. (2015). Two magma bodies
230   beneath the summit of Kīlauea Volcano unveiled by isotopically distinct melt deliveries
231   from the mantle. *Earth and Planetary Science Letters* **413**, 90–100.

232 Pietruszka, A. J., Marske, J. P., Heaton, D. E., Garcia, M. O. & Rhodes, J. M. (2018). An Isotopic
233   Perspective into the Magmatic Evolution and Architecture of the Rift Zones of Kīlauea
234   Volcano. *Journal of Petrology* **59**, 2311–2352.

235 Re, G., Corsaro, R. A., D'Oriano, C. & Pompilio, M. (2021). Petrological monitoring of active
236   volcanoes: A review of existing procedures to achieve best practices and operative
237   protocols during eruptions. *Journal of Volcanology and Geothermal Research* **419**,
238   107365.

239 Ryan, M. P. (1987). The elasticity and contractancy of Hawaiian olivine tholeiite, and its role in
240   the stability and structural evolution of sub-caldera magma reservoirs and rift systems. In
241   Volcanism in Hawaii. *US Geol. Surv. Prof. Pap.* **1350**, 1395–1447.

242 Span, R. & Wagner, W. (1996). A new equation of state for carbon dioxide covering the fluid
243   region from the triple-point temperature to 1100 K at pressures up to 800 MPa. *Journal of
244   physical and chemical reference data*. American Institute of Physics for the National
245   Institute of Standards and … **25**, 1509–1596.

246 Welsch, B., Faure, F., Famin, V., Baronnet, A. & Bachèlery, P. (2013). Dendritic Crystallization:
247   A Single Process for all the Textures of Olivine in Basalts? *Journal of Petrology* **54**, 539–
248   574.

249 Wieser, P. E. *et al.* (2021). Reconstructing Magma Storage Depths for the 2018 Kīlauean
250   Eruption From Melt Inclusion CO2 Contents: The Importance of Vapor Bubbles.
251   *Geochemistry, Geophysics, Geosystems* **22**, e2020GC009364.

252   Wieser, P. E., Edmonds, M., Maclennan, J., Jenner, F. E. & Kunz, B. E. (2019). Crystal
253   scavenging from mush piles recorded by melt inclusions. *Nature Communications*.
254   Nature Publishing Group **10**, 5797.

255   Wieser, P. E., Kent, A. J. R. & Till, C. B. (2023a). Barometers Behaving Badly II: a Critical
256   Evaluation of Cpx-Only and Cpx-Liq Thermobarometry in Variably-Hydrous Arc
257   Magmas. *Journal of Petrology* **64**, egad050.

258   Wieser, P. E., Kent, A., Till, C. & Abers, G. (2023b). Geophysical and Geochemical Constraints
259   on Magma Storage Depths along the Cascade Arc: Knowns and Unknowns. EarthArXiv.

260

261

262   **Figure captions**

263

264   **Figure 1. Workflow of the study, all times on this figure are Pacific Standard Time (PST).**

265   Stick people show the contribution of individual team members, to indicate the total time associated

266   with each step. We note that AB was trained in these procedures during the simulation and all

267   reports were sent to HVO prior to 5:30 pm Hawaii Standard Time (HST), thus allowing for decision

268   making for the following day.

269

270   **Figure 2. Evolution of results over 4 days.** a) Schematic model of Kīlauea's plumbing

271   system, indicating reservoir depths determined by geophysics and prior petrological work

272   (HMM- Halemaʻumaʻu; SC – South Caldera). b) By the end of Day 1, FI revealed that the

273   crystals were supplied from depths consistent with the Halemaʻumaʻu reservoir.

274   Kolmogorov-Smirnov tests show that September 2023 FI are recording depths significantly

275   shallower than those recorded by FI (critical D = 0.22, stat = 0.24, pval=0.016) and MI (critical

276   D = 0.22, stat = 0.41, pval=3.51e-06) from the 2018 lower East Rift Zone eruption, which required

277   a contribution from the South Caldera reservoir. [1] Melt inclusion data for the 2018 LERZ eruption

278   is from Wieser *et al.*, (2021); [2] Fluid inclusion data for the 2018 LERZ eruption is from DeVitre

279   and Wieser, (2023) c) By the end of Day 2, depths from 46 FI were sent to HVO, confirming a

280   dominant role of the Halemaʻumaʻu reservoir. On Day 2 we applied a conservative degassing filter

281   (SO_2 mol% < 2.5). d) By the end of Day 4, after taking a mean of repeated analyses of single FI,

282   applying more stringent data filters, using FI-specific temperatures, and a more appropriate crustal

283   model (density of ~2300 kg/m^3 with a normal error distribution of 100 kg/m^3), entrapment depths

284   with uncertainties were linked to crystal chemistry. Error bars correspond to uncertainties

285   propagated using Monte Carlo simulations (see Supplementary Information S1 Appendix)

* The use of trade names does not signify endorsement by the U.S. Geological Survey.

286   Olivine Fo equilibrium field is calculated based on Glass EPMA data collected on September 11,

287   2023 (see Supplementary Information S1 Appendix). We note here that initial data for Days 1

288   and 2 did not filter out repeated analyses (1 repeated FI in Day 1 and 6 in Day 2), pressures were

289   calculated using an estimated entrapment temperature of 1150˚C (Wieser *et al.*, 2021; DeVitre and

290   Wieser, 2023), and depth was calculated using the model of (Ryan, 1987) described in (Lerner *et*

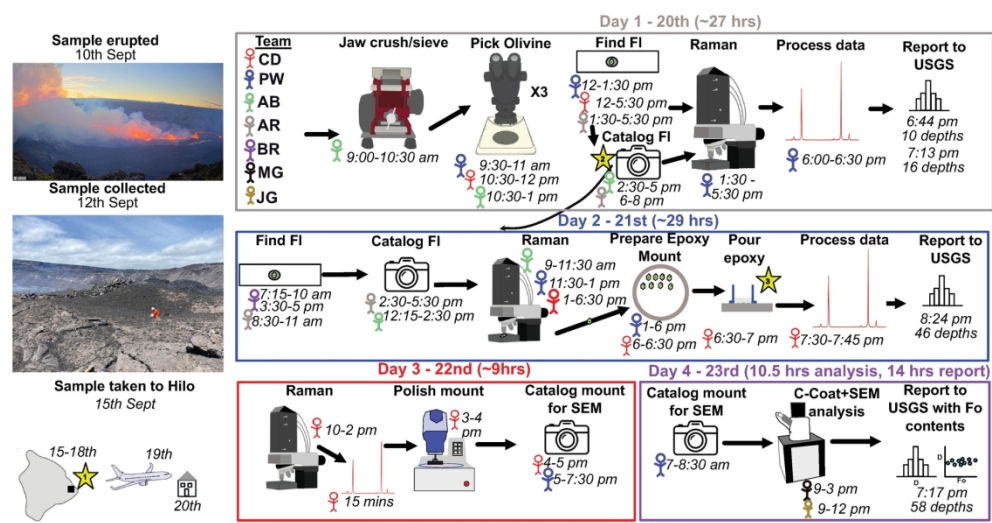291   *al.*, 2021) for crustal density.

292

293

Figure 1. Workflow of the study, all times on this figure are Pacific Standard Time (PST). Stick people show the contribution of individual team members, to indicate the total time associated with each step. We note that AB was trained in these procedures during the simulation and all reports were sent to HVO prior to 5:30 pm Hawaii Standard Time (HST), thus allowing for decision making for the following day.
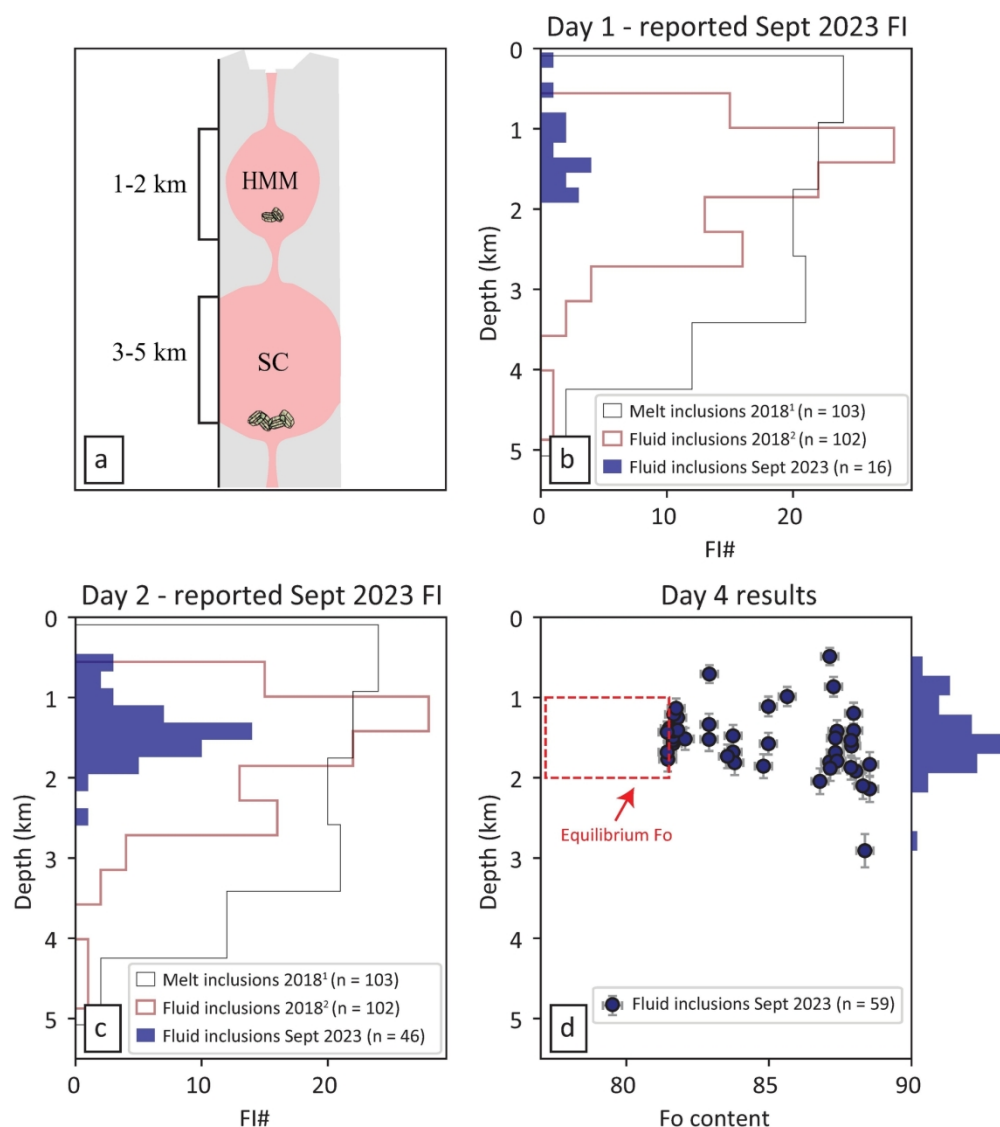
168x87mm (300 x 300 DPI)

Figure 2. Evolution of results over 4 days. a) Schematic model of Kīlauea's plumbing system, indicating reservoir depths determined by geophysics and prior petrological work (HMM- Halemaʻumaʻu; SC – South Caldera). b) By the end of Day 1, FI revealed that the crystals were supplied from depths consistent with the Halemaʻumaʻu reservoir. Kolmogorov-Smirnov tests show that September 2023 FI are recording depths significantly shallower than those recorded by FI (critical D = 0.22, stat = 0.24, pval=0.016) and MI (critical D = 0.22, stat = 0.41, pval=3.51e-06) from the 2018 lower East Rift Zone eruption, which required a contribution from the South Caldera reservoir. 1 Melt inclusion data for the 2018 LERZ eruption is from Wieser et al., (2021); 2 Fluid inclusion data for the 2018 LERZ eruption is from DeVitre and Wieser, (2023) c) By the end of Day 2, depths from 46 FI were sent to HVO, confirming a dominant role of the Halemaʻumaʻu reservoir. On Day 2 we applied a conservative degassing filter (SO2 mol% < 2.5). d) By the end of Day 4, after taking a mean of repeated analyses of single FI, applying more stringent data filters, using FI-specific temperatures, and a more appropriate crustal model (density of ~2300 kg/m3 with a normal error distribution of 100 kg/m3), entrapment depths with uncertainties were linked to crystal chemistry. Error bars correspond to uncertainties propagated using Monte Carlo simulations (see Supplementary Information S1 Appendix) Olivine Fo equilibrium field is calculated based on Glass EPMA data

collected on September 11, 2023 (see Supplementary Information S1 Appendix). We note here that initial data for Days 1 and 2 did not filter out repeated analyses (1 repeated FI in Day 1 and 6 in Day 2), pressures were calculated using an estimated entrapment temperature of 1150˚C (Wieser et al., 2021; DeVitre and Wieser, 2023), and depth was calculated using the model of (Ryan, 1987) described in (Lerner et al., 2021) for crustal density.

166x186mm (300 x 300 DPI)